

Sub-barrier fusion of Si+Si systems

G. Colucci^{1,*}, G. Montagnoli¹, A. M. Stefanini², D. Bourgin⁴, P. Čolović⁵, L. Corradi², S. Courtin⁴, M. Faggian¹, E. Fioretto³, F. Galtarossa^{2,6}, A. Goasduff², F. Haas⁴, M. Mazzocco¹, F. Scarlassara¹, C. Stefanini¹, E. Strano¹, M. Urbani¹, S. Szilner⁵, and G. L. Zhang²

¹Dipartimento di Fisica e Astronomia, Università di Padova, and INFN, I-35131 Padova, Italy

²INFN, Laboratori Nazionali di Legnaro, I-35020 Legnaro, Italy

³IPHC, CNRS-IN2P3, Université de Strasbourg, F-67037 Strasbourg Cedex 2, France

⁴Ruder Bošković Institute, HR-10002 Zagreb, Croatia

⁵Dipartimento di Fisica e Scienze della Terra, Univ. di Ferrara, Ferrara, Italy

Abstract. The near- and sub-barrier fusion excitation function has been measured for the system $^{30}\text{Si}+^{30}\text{Si}$ at the Laboratori Nazionali di Legnaro of INFN, using the ^{30}Si beam of the XTU Tandem accelerator in the energy range 47 - 90 MeV. A set-up based on a beam electrostatic deflector was used for detecting fusion evaporation residues. The measured cross sections have been compared to previous data on $^{28}\text{Si}+^{28}\text{Si}$ and Coupled Channels (CC) calculations have been performed using M3Y+repulsion and Woods-Saxon potentials, where the low-lying 2^+ and 3^- excitations have been included. A weak imaginary potential was found to be necessary to reproduce the low energy $^{28}\text{Si}+^{28}\text{Si}$ data. This probably simulates the effect of the oblate deformation of this nucleus. On the contrary, ^{30}Si is a spherical nucleus, $^{30}\text{Si}+^{30}\text{Si}$ is nicely fit by CC calculations and no imaginary potential is needed. For this system, no maximum shows up for the astrophysical S-factor so that we have no evidence for hindrance, as confirmed by the comparison with CC calculations. The logarithmic derivative of the two symmetric systems highlights their different low energy trend. A difference can also be noted in the two barrier distributions, where the high-energy peak present in $^{28}\text{Si}+^{28}\text{Si}$ is not observed for $^{30}\text{Si}+^{30}\text{Si}$, probably due to the weaker couplings in last case.

1 Introduction

It is well known that nuclear structure strongly influences fusion reaction dynamics at energies near and below the Coulomb barrier. The comparison of data for neighboring isotopes is a sensitive tool to evidence this influence.

Through the application of this method it has been possible to discover the influence of transfer channels on fusion reactions, as in Ni + Ni [1, 2] and Ca + Ca [3] systems, and the effect of changing structure from spherical to strongly deformed nuclei, as in $^{16}\text{O} + ^{148,154}\text{Sm}$ [4, 5].

A similar comparative study has been performed also for the Si+Si systems [6], where the interest originates from the different shape of the silicon isotopes: ^{30}Si is nearly spherical, whereas ^{28}Si is strongly deformed with an oblate shape. Previous studies [6, 7] revealed the influence of transfer on fusion of the asymmetric system $^{28}\text{Si}+^{30}\text{Si}$ which has been explained by considering one- and successive two-neutron transfer channels in the coupling scheme.

The excitation functions of $^{28}\text{Si}+^{28}\text{Si}$ and $^{30}\text{Si}+^{30}\text{Si}$ have different trends (see Fig. 1a). The case of $^{28}\text{Si}+^{28}\text{Si}$ involving deformed nuclei shows an unusual behaviour, where the cross section is hindered just below the barrier and then enhanced at lower energies, as shown in the compar-

ison with the CC calculations of Fig. 1b. It was further surprising that the low-energy data were well reproduced only by artificially applying a weak, short-ranged imaginary potential, probably simulating the effect of the oblate deformation. This feature has to be further investigated and a complete study of $^{30}\text{Si}+^{30}\text{Si}$ appeared to be very important in this respect.

The spherical shape of ^{30}Si together with the absence of transfer channels with positive Q-values allows to only consider couplings to the vibrational states. The lack of experimental fusion data below 4 mb for $^{30}\text{Si}+^{30}\text{Si}$ prevented a meaningful comparison between the two systems. Therefore, a fusion experiment has been recently carried out at Laboratori Nazionali di Legnaro (LNL) with the purpose to extend the data of $^{30}\text{Si}+^{30}\text{Si}$ down to energies deeply below the Coulomb barrier.

In this contribution we present the results of this full measurement from well below to well above the Coulomb barrier, and we perform a comparison with the existing data for the $^{28}\text{Si}+^{28}\text{Si}$ system.

2 Experimental set-up

Fusion cross sections for the $^{30}\text{Si}+^{30}\text{Si}$ system have been determined by direct detection of the evaporation residues (ER) at very forward angles by exploiting their different

*e-mail: giulia.colucci@studenti.unipd.it

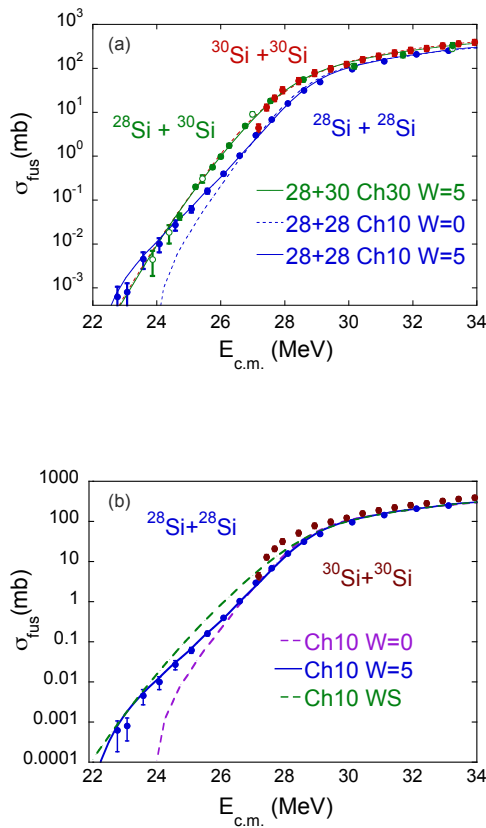


Figure 1: (a) Measured fusion excitation function of $^{28}\text{Si} + ^{28}\text{Si}$, $^{28}\text{Si} + ^{30}\text{Si}$ [6] and previous data for $^{30}\text{Si} + ^{30}\text{Si}$ [8]; the lines are the results of CC calculations. (b) Comparison of $^{28}\text{Si} + ^{28}\text{Si}$ with CC calculations involving a Woods-Saxon potential (Ch10 WS) and a double folding M3Y+rep. potential with (Ch10 w5) and without (Ch10 w0) an imaginary short ranged potential.

electrical rigidity with respect to beam and beam-like particles, using an electrostatic deflector. This experimental set-up is shown in Fig. 2, it allows fast and reliable measurements of relative and absolute cross sections and has been employed in several sub- and near-barrier fusion experiments at LNL in recent years. A subsequent E-TOF- ΔE telescope allows the ER identification. This telescope consists of two micro-channel plate (MCP) detectors, a transverse field ionization chamber (IC) and a silicon detector placed in the same gas (CH_4) volume. The IC provides an energy loss signal ΔE , while the two MCPs yield the time of flights (TOF) together with the silicon detector. In this configuration the silicon detector measures the residual energy of the ER and gives both the trigger for data acquisition and the start signal for the TOF. Typical spectra of TOF as a function of the residual energy E are shown in Fig. 3, where a good separation of ER events from the residual beam can be appreciated at energies both above and below the Coulomb barrier. Analogous two-dimensional spectra of TOF vs. ΔE and ΔE vs. E were used in the data analysis.

Four silicon detectors were placed symmetrically at $\theta_{\text{lab}} = 16^\circ$ around the beam direction, in the sliding seal reaction chamber. These detectors were used to monitor the beam and normalize to the Mott scattering cross section. The XTU Tandem accelerator at LNL provided ^{30}Si beams in the energy range of 47-90 MeV, with intensities of 15-30 pA. The targets consisted of $50 \mu\text{g}/\text{cm}^2$ metallic ^{30}Si evaporated on $30 \mu\text{g}/\text{cm}^2$ carbon backings facing the beam. The isotopic enrichment of ^{30}Si was 99.64 %, where the small amounts of ^{29}Si and ^{28}Si did not affect the fusion cross section because of their higher Coulomb barriers. The carbon backing and the silicon target itself introduced an average beam energy loss of around 750-850 keV, which was taken into account in the analysis. Three ER angular distributions were measured at the energies of 58, 72 and 80 MeV in the range from -6° to $+9^\circ$. The total fusion cross section was derived by integrating those distributions, and by simple interpolations or extrapolations for all other energies, where measurements were taken only at 2° (or 3° for low energies). The measured energy range allowed to extend the excitation function down to $\approx 4 \mu\text{b}$, as shown Fig. 4a. The reported errors are statistical uncertainties, which are 1-2 % at the higher energies and increase to 10-20 % at energies below the barrier. The systematic errors on the absolute cross sections are estimated $\pm 7-8 \%$, due to the geometrical solid angle uncertainties, angular distribution integrations and mainly to the deflector transmission. The fusion cross sections of $^{30}\text{Si} + ^{30}\text{Si}$ and $^{28}\text{Si} + ^{28}\text{Si}$ are reported in Fig. 4b. From this first comparison it appears that the two excitation functions behave differently at low energies with a flatter slope for $^{28}\text{Si} + ^{28}\text{Si}$. A CC analysis has been performed to understand the origin of this difference.

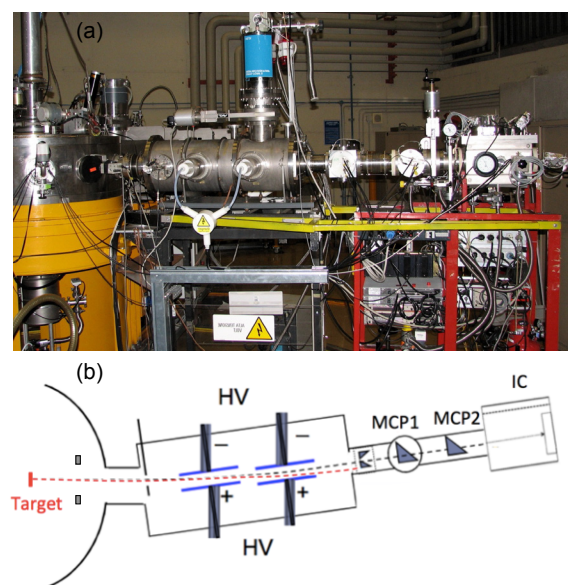


Figure 2: The experimental set-up (a) and its scheme (b). The reaction chamber, the electrostatic deflector and the telescope E-TOF- ΔE are drawn from the left.

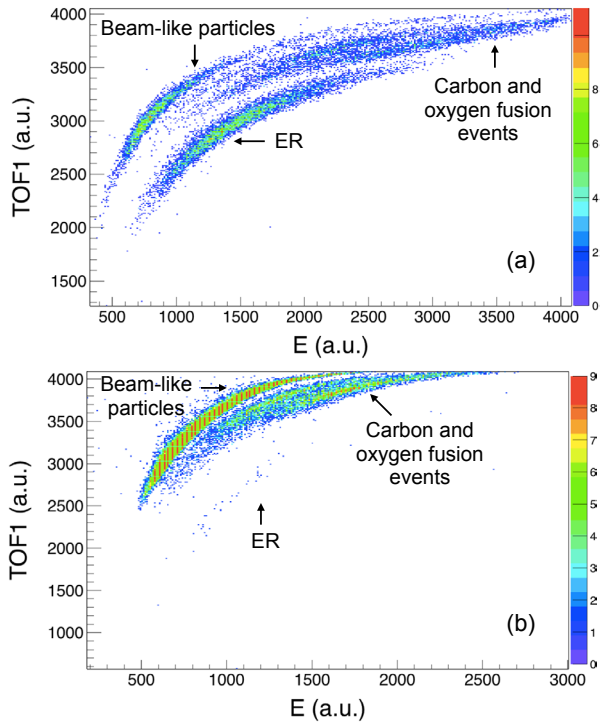


Figure 3: Time of flight TOF1 (ordinate) as a function of the residual energy E (abscissa). The spectra were obtained above the Coulomb barrier (80 MeV, $\sigma_{fus}=527$ mb, (a) and at a sub-barrier energy of 50 MeV ($\sigma_{fus}=115 \mu b$, (b)). We can see, besides fusion events from $^{30}\text{Si}+^{30}\text{Si}$ and beam-like particles, the residues produced by the fusion of ^{30}Si with the carbon and oxygen present in the target.

3 Coupled channel calculations

The CC analysis of the sub-barrier excitation function employed, in a first step, a double-folding M3Y+repulsion potential [9]. The calculation makes use of the isocentrifugal approximation and includes one- and two-phonon vibrational modes as well as mutual excitations of the low-lying 2^+ and 3^- states in both projectile and target (this calculation is called Ch10 in Fig. 5). The adopted coupling strengths are reported in Table I of Ref. [6].

The ^{30}Si nucleus is nearly spherical, indeed the measured quadrupole moment of the 2^+ state is $Q_2 = -0.05(6)$ b, which is consistent with zero. As a consequence, the location of minimum of channels potentials is essentially the same in all channels, as discussed in detail in Ref. [6]. As anticipated in Sec. 2, the two excitation functions of $^{28}\text{Si}+^{28}\text{Si}$ and $^{30}\text{Si}+^{30}\text{Si}$ have different trends below the barrier. This difference was suggested to be due to the different shape of the two silicon isotopes. The effect of the oblate deformation of ^{28}Si was simulated in Ref. [6] by applying a weak imaginary potential at small ion-ion distances (inside the Coulomb barrier), and this allowed to obtain a good data fit. On the contrary, it appears that in the case of $^{30}\text{Si}+^{30}\text{Si}$ no imaginary potential is needed below the barrier, simply because that nucleus is spherical. This is shown in Fig. 5a where the results of CC calculations without and with the imaginary potential are reported. It

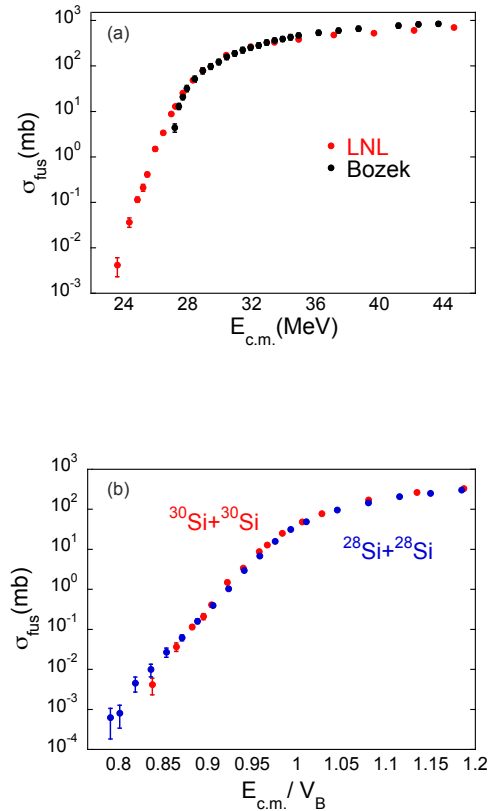


Figure 4: Fusion excitation function of $^{30}\text{Si}+^{30}\text{Si}$ compared to previous experimental data [8] (a) and to the $^{28}\text{Si}+^{28}\text{Si}$ system (b).

is evident that there is essentially no difference between the two calculations.

4 Barrier distributions

Fusion barrier distributions [10] often give a significant insight into the role of the target and projectile structure. Therefore the barrier distribution of $^{30}\text{Si}+^{30}\text{Si}$ has been extracted and compared to the one of $^{28}\text{Si}+^{28}\text{Si}$ in order to obtain more information on the possible role of the deformation of ^{28}Si .

The barrier distributions were obtained using the three-point difference formula [11], with two energy steps of 1.0 MeV and 1.5 MeV, and a meaningful difference between the two systems has been observed. This is shown in Fig. 6, where $^{30}\text{Si}+^{30}\text{Si}$ has a single well-defined peak, while a double-peak structure appears for $^{28}\text{Si}+^{28}\text{Si}$ with a clearly defined high-energy peak. These dissimilar behaviours arise from the different structures of the two nuclei and from the stronger couplings present in $^{28}\text{Si}+^{28}\text{Si}$ due to the oblate shape of ^{28}Si .

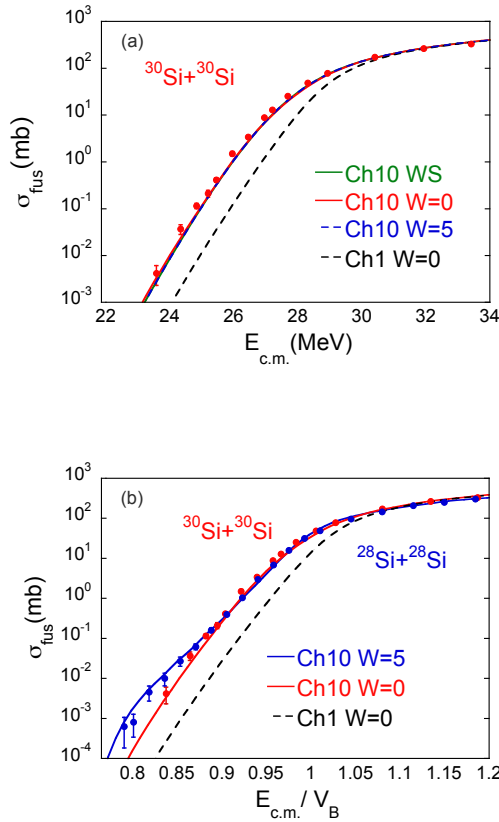


Figure 5: (a) Measured fusion cross section for $^{30}\text{Si}+^{30}\text{Si}$ compared to the no-coupling limit and to the CC calculations, based on three different potentials: a Woods-Saxon potential (Ch10 WS), and a M3Y+rep. potential with (Ch10 W5) and without (Ch10 W0) an imaginary potential. (b) Comparison of $^{30}\text{Si}+^{30}\text{Si}$ with $^{28}\text{Si}+^{28}\text{Si}$. CC Calculations for the second system [6] are also reported, based on a M3Y+rep. potential with an imaginary part.

5 Hindrance

Hindrance is a suppression of fusion cross section with respect to standard CC calculations, occurring far below the Coulomb barrier [12, 13]. The investigation of hindrance usually makes use of two model-independent representations of the excitation functions which allow to reveal the presence of the phenomenon: the astrophysical S-factor [14] and the logarithmic derivative $L(E)$. Indeed, the S factor shows a maximum vs. energy in the presence of hindrance at the energy where the logarithmic slope $L(E)$ of the excitation function reaches the value L_{CS} expected for a constant astrophysical S factor.

In the case of $^{30}\text{Si}+^{30}\text{Si}$ the S factor does not show any maximum vs. energy (see Fig. 7b), even if it appears to saturate at the lowest measured energies and the logarithmic derivative does not cross the L_{CS} curve (Fig. 7a). These features suggested the absence of hindrance in the measured energy range, but a confirmation was necessary. Indeed, it has been pointed out that in systems

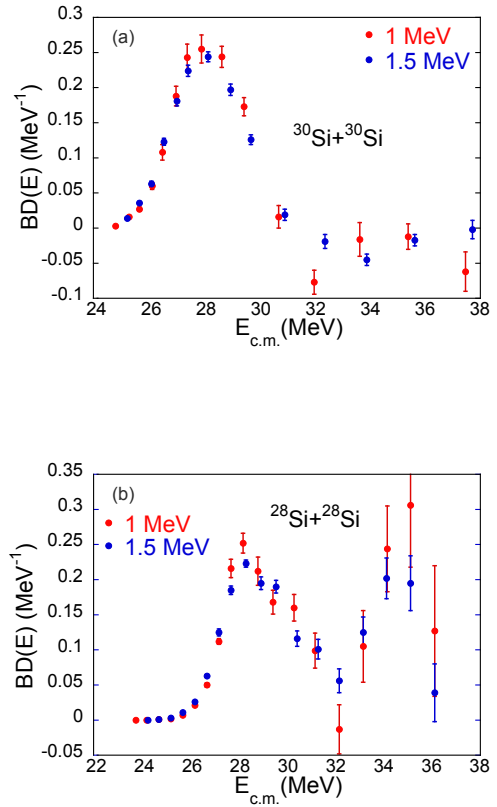


Figure 6: Barrier distributions extracted for $^{30}\text{Si}+^{30}\text{Si}$ (a) and $^{28}\text{Si}+^{28}\text{Si}$ (b), with energy steps of 1.0 MeV (red points) and 1.5 MeV (blue points).

with a positive Q-value for fusion the S factor does not necessarily develop a maximum [13]. A comparison with the theoretical model was then performed by CC calculations with a standard Woods-Saxon potential. These calculations nicely fit the experimental excitation function, as can be seen in Fig. 5a. The analogous calculations using the M3Y+rep. potential give very similar results. It is evident that the excitation function is not suppressed at energies below the Coulomb barrier, so that there is no evidence of hindrance down to around $4 \mu\text{b}$.

6 Summary

The fusion excitation function of $^{30}\text{Si}+^{30}\text{Si}$ has been measured in a wide energy range down to $4 \mu\text{b}$. The comparison with $^{28}\text{Si}+^{28}\text{Si}$ shows that the two systems behave differently near the barrier where the high energy peak observed in the barrier distribution of $^{28}\text{Si}+^{28}\text{Si}$ is not found for $^{30}\text{Si}+^{30}\text{Si}$.

Below the barrier the heavier system exhibits a regular trend in contrast with the unusual behaviour of $^{28}\text{Si}+^{28}\text{Si}$. The weaker couplings in $^{30}\text{Si}+^{30}\text{Si}$ and its spherical shape could be responsible for this difference. This is confirmed by CC calculations using the M3Y+rep. and a

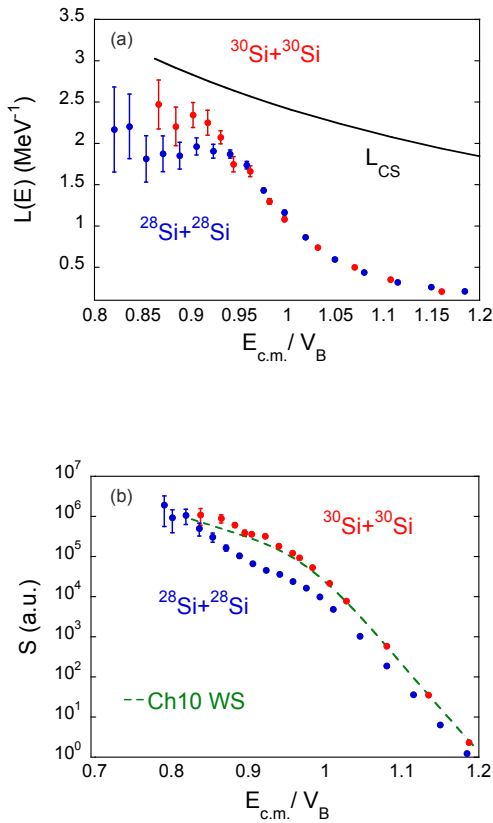


Figure 7: (a) Logarithmic derivative of the excitation function of the two systems, where L_{CS} (black line) is the slope expected for a constant astrophysical S-factor. (b) S-factor extracted from experimental data for both cases and, for $^{30}\text{Si}+^{30}\text{Si}$, from CC calculations based on a Woods - Saxon potential (green line), well reproducing the data.

Woods-Saxon potential, that are in good agreement with experimental data. At variance with the case of $^{28}\text{Si}+^{28}\text{Si}$,

adding a weak short-ranged imaginary potential is not necessary to reproduce the sub-barrier fusion cross sections of $^{30}\text{Si}+^{30}\text{Si}$. When observing the logarithmic slope of the excitation function and the S-factor, there is no evidence for hindrance in the measured energy range for this system.

7 Acknowledgments

The collaboration with H.Esbensen who performed the CC calculations with the M3Y+rep. potential is gratefully acknowledged. This work has been supported in the part by the Croatian Science Foundation under the project 7194.

References

- [1] M. Beckerman, M. Salomaa, A. Sperduto, J. D. Moltoris, and A. Di Rienzo, *Phys. Rev. C* **25**, 837 (1982).
- [2] M. Beckerman et al., *Phys. Rev. Lett.* **45**, 1472 (1980).
- [3] G. Montagnoli et al., *Phys. Rev. C* **85**, 024607 (2012).
- [4] R. Stokstad et al., *Z. Phys. A* **295**, 269 (1980).
- [5] H. Esbensen, *Nucl. Phys. A* **352**, 147 (1982).
- [6] G. Montagnoli et al., *Phys. Rev. C* **90**, 044608 (2014).
- [7] C. L. Jiang, et al., *Phys. Rev. C* **78**, 017601 (2008).
- [8] E. Bozek et al., *Nucl. Phys. A* **451**, 171 (1986).
- [9] Ş. Mişicu and H. Esbensen, *Phys. Rev. C* **75**, 034606 (2007).
- [10] N. Rowley, G. R. Satchler, and P. H. Stelson, *Phys. Lett. B* **254**, 25 (1991).
- [11] H. Timmers et al., *Nucl. Phys. A* **633**, 421 (1998).
- [12] C. L. Jiang, et al., 2002, *Phys. Rev. Lett.* **89**, 052701(2002).
- [13] C. L. Jiang, H. Esbensen, B. B. Back, R. V. F. Janssens, and K. E. Rehm, *Phys. Rev. C* **69**, 014604 (2004).
- [14] E. M. Burbidge, G. Burbidge, W. Fowler, and F. Hoyle, *Rev. Mod. Phys.* **29**, 547 (1957).